IEEE Access
Multidisciplinary | Rapid Review | Open Access Journal

Received April 18, 2020, accepted May 4, 2020, date of publication May 21, 2020, date of current version June 2, 2020.

Digital Object Identifier 10.1109/ACCESS.2020.2996432

Quantification of Atherosclerotic Plaque Elasticity Using Ultrasonic Texture Matching

HONGYU KANG[1,2], (Member, IEEE), YANLING ZHANG[3], XIAOWEI HUANG[1], (Member, IEEE), LILI NIU[1], (Member, IEEE), HUI ZHANG[3], LISHENG XU[2], (Senior Member, IEEE), AND DEREK ABBOTT[4,5], (Fellow, IEEE)

[1]Paul C. Lauterbur Research Center for Biomedical Imaging, Institute of Biomedical and Health Engineering, Shenzhen Institutes of Advanced Technology, Chinese Academy of Sciences, Shenzhen 518055, China
[2]College of Medicine and Biological Information Engineering, Northeastern University, Shenyang 110819, China
[3]Department of Ultrasound, Third Affiliated Hospital, Sun Yat-sen University, Guangzhou 510630, China
[4]Centre for Biomedical Engineering, University of Adelaide, Adelaide, SA 5005, Australia
[5]School of Electrical and Electronic Engineering, University of Adelaide, Adelaide, SA 5005, Australia

Corresponding authors: Hui Zhang (zhang9@mail.sysu.edu.cn), Lisheng Xu (xuls@bmie.neu.edu.cn), and Derek Abbott (derek.abbott@adelaide.edu.au)

This work was supported in part by the National Key Research and Development Program of China under Grant 2016YFC0104700, in part by the National Science Foundation (NSFC) under Grant 81701713, Grant 11774371, Grant 11674347, Grant 61773110, and Grant 61374015, in part by the Guangdong Grant ''Key Technologies for Treatment of Brain Disorders'' under Grant 2018B030332001 and Grant 2018B030331001, in part by the Youth Innovation Promotion Association CAS under Grant 2018393 and Grant 2020358, and in part by the Natural Science Foundation of Guangdong Province under Grant 2016TQ03X716 and Grant 2016TQ03R472.

ABSTRACT The composition of an atherosclerotic plaque is a major determinant of its vulnerability, i.e. proneness to rupture. This paper proposes an ultrasonic texture matching method, which is shown to reflect the distribution of elastic modulus and is a potential method for quantitatively analyzing different plaque components based on B-mode cine-loops. We performed an *in vitro* study, employing plaque phantoms fabricated using polyvinyl alcohol. Firstly, the phantoms with two components (soft tissue: 60.9 ± 6.8 kPa; surrounding tissue: 248.8 ± 12.1 kPa) were fabricated. Soft tissue occupied 10%, 40% and 64% of the total plaque volume. Further, three tissue components (soft tissue: 60.9 ± 6.8 kPa; hard tissue: 248.8 ± 12.1 kPa; surrounding tissue: 310.3 ± 14.1 kPa) were made. Soft and hard tissues occupied 32% of total plaque volume, respectively. For our *in vivo* study, six mice with ApoE knockout and three New Zealand white rabbits with abdominal aortic balloon injury were evaluated. Ultrasound cine-loop data of plaques were collected to calculate elastic modulus, then the plaque tissues were removed for further histology examination. The cine-loop data *in vitro* study and *in vivo* study were acquired by an ultrasound micro-imaging system (VisualSonics Vevo2100). In the phantom experiment, the mean elastic moduli of two component phantoms were 60.4 ± 7.6 kPa (soft tissue) and 198.5 ± 12.5 kPa (surrounding tissue), respectively. Similarly, the mean elastic moduli of three component phantoms exhibited 90.2 ± 6.2 kPa (soft tissue), 184.3 ± 11.6 kPa (hard tissue) and 381.6 ± 3.8 kPa (surrounding tissue), respectively. In animal experiments, the percentage of lipid tissue and calcification regions was also quantified in mice and in rabbit experiment with the histological results. This suggests that the texture matching method may be a potential method to identify lipid component of plaque and to predict the vulnerability of atherosclerosis plaques noninvasively.

INDEX TERMS Ultrasound imaging, plaque, biomechanics, elastic modulus.

I. INTRODUCTION

Cardiovascular disease (CVD) has caused serious health problems and results in an economic burden all over the world [1]. Intravascular plaque rupture is one of dominant reasons for cardiovascular events [2]. Vulnerable plaques usually are described as having a large lipid core and a thin fibrous cap, which are proposed as an important determinant for their detection [3]–[5]. Post-mortem studies in patients who exhibited fatal coronary events suggest that large lipid core plaques cause most coronary events [6]. Therefore, it is important to accurately identify and quantify plaque

The associate editor coordinating the review of this manuscript and approving it for publication was Jenny Mahoney.

components, especially, soft tissue components (large lipid core) for predicting vulnerable plaque before rupture in a clinical setting.

Various diagnostic invasive methods have been investigated to identify plaque components. Intravascular ultrasound (IVUS) was proposed for distinguishing plaques morphology [7], [8]. Intravascular ultrasound elastography (IVUSE) is a technique based on IVUS [9], [10], which can be used to qualify or quantify specific histologic components of atherosclerotic plaques by measuring tissue elastic properties to identify vulnerable plaques [11]–[13]. Virtual-histology intravascular ultrasonography (VH-IVUS) [14], [15] was widely used to qualitatively identify coronary plaque specific components including fibrous tissue, fatty tissue, necrotic core and calcification [16], [17]. Optical coherence tomography (OCT) was widely used for coronary plaque characterization [18], [19], especially the detection of thin-cap fibro atheroma caused plaque rupture [20]–[22]. Moreover, OCT characterizations for various plaque components such as lipid content, fibrous cap thickness and calcification were also validated by histology [23], [24]. Computed tomography is also a technology for detecting the component of atherosclerotic plaques, but it also has limitation to evaluate necrotic core and underestimate calcification (Weert, *et al.* 2006, Obaid, *et al.* 2013). Though these techniques were capable of distinguishing the characteristics and components of the atherosclerotic plaques, their invasive nature presents a limitation.

Magnetic Resonance Elastography (MRE) is a noninvasive technology for quantitatively assessing the mechanical properties of tissue, especially for application to estimate the stiffness of organs such as brain, breast, blood vessel, heart, kidney, lung, and skeletal muscle [25]–[28]. In addition, Magnetic Resonance Imaging (MRI) combined with T2 mapping can be used to discriminate tissue characteristics and plaque components with desired accuracy in comparison with histology [29]–[31]. However, MRI is very expensive for widespread use and also time consuming. Moreover, the capability of Positron Emission Tomography (PET) for quantification of plaque inflammation has been evaluated to predict the risk of atherosclerotic plaque rupture, but the disadvantage is that contrast agents are required and the human body is exposed to radiation [32], [33].

Ultrasound examination is a common and non-invasive technique for detecting the pathology of internal body structures such as tendons, muscles, joints, blood vessels, and internal organs. Recently, ultrasound techniques were developed to identify the vulnerability of the plaque with the advantage of being inexpensive and non-invasive. Noninvasive ultrasound techniques based on radiofrequency (RF) data were used to estimate the strain of plaques [34]–[36]. Roy Cardinal *et al.* reported that ultrasound noninvasive vascular elastography (NIVE) based on RF data is able to quantify axial strain, shear strain, and translation motion. Thirty-one patients were enrolled in the study, and the results showed that ratio of cumulated axial strain to cumulated axial translation of vulnerable plaque were apparently higher than nonvulnerable plaques without neovascularity [37].

Kanai *et al.* provided a noninvasive method based on envelope data for evaluating the regional elasticity of tissue surrounding atherosclerotic plaque. Nine iliac arteries with plaques were used in the experiment and the elasticity of plaques were shown to be about 81 ± 40 kPa and 1.0 ± 0.63 MPa, which were used as the reference parameters [38]. However, the limitation was that the amount of RF data was large and the process of calculation was time consuming. Widman *et al.* adopted a developed speckle tracking (ST) algorithm based on B-mode, which was used to assess plaque strain and was verified in phantoms and *in vivo* using sonomicrometry. For the *in vitro* and *in vivo* results, radial and longitudinal limits of agreement (LOA) were well correlated and occurred between ST and sonomicrometry peak strains [39]. Shear wave elastography (SWE) can also be a measure to quantify elastic modulus distribution in atherosclerotic plaque. However, the reproducibility, accuracy and resolution of the SWE technique needs to be further improved [40]–[43].

Vulnerable plaques usually have a large lipid core that is an important determinant for detection. The aim of our study is to use the proposed texture matching method to quantitatively analyze the elastic modulus distribution and identifies lipid components in plaques. The method is potentially a noninvasive method to evaluate the vulnerability of atherosclerotic plaque based on B-mode images. The B-mode data can be acquired easily in clinical ultrasound equipment and is inexpensive and non-invasive. The feasibility of this method was demonstrated using *in vitro* plaque phantoms made from polyvinyl alcohol (PVA) cryogel and *in vivo* animal abdominal aortic plaques.

II. MATERIALS AND METHODS

A. THE TEXTURE MATCHING METHOD

Our study provides a texture matching method to calculate the distribution of elastic distribution of plaques. The procedures of the method are as follows: firstly, $f^{(1)}(x, y), \ldots, f^{(N)}(x, y)$ are N frames of B-mode images extracted from a cine-loop, where (x, y) corresponds to the coordinates of a pixel in the image plane. Then, $g^{(n)}(x, y)$ and $g^{(n+1)}(x, y)$ are selected from two successive images $f^{(n)}(x, y)$ and $f^{(n+1)}(x, y)$ $(1 < n < N)$ are defined as the region-of-interest (ROI), and ROI is a rectangular area that contains the entire plaque. The texture matching method starts when $n = 1$ and repeats with the same size ROI translated exactly the same distance as the estimated displacement, until $n = N - 1$. Here, the RIO is the target region for calculating the elastic modulus distribution. Each ROI is divided into a grid of small sections known as interrogation windows. After a series of interrogation windows are divided, the most similar texture distribution of interrogation windows of two consecutive B-mode images are matched. The texture displacement of each interrogation

window is obtained via a normalized two-dimensional cross-correlation algorithm with sub-pixel method, filter and interpolation method, and these methods have been explained in our previous studies [44], [45].

For improving the accuracy of displacement, the Gaussian peak fitting is used for the sub-pixel analysis. Then, in the displacement field, the vector will be erased if it is larger than the median of all the nine vectors plus the threshold (1.7–3.0) times the standard deviation of all the vectors, or if it is smaller than the median minus the threshold times the standard deviation when each vector is compared to the eight vectors surrounding it.

The filtering is used to modify the non-uniform vectors. The bilinear interpolation method is used to supplement the missing vector, and the rotation and deformation of ROIs in the images are calculated by the gradient of the two-dimensional translational displacement described above. Two-dimensional displacement $v(x, y, n)$ of the geometric transformation is acquired, where x and y are image coordinates, and n is the frames of B-mode images.

A previous detailed description of the algorithms has been reported by our previous studies [44], [45]. All the algorithms are implemented in Matlab (64-bit, R2016b, MathWorks Inc., Natick, MA, USA).

B. ELASTIC MODULUS EVALUATION

After the estimated displacements $v(x, y, n)$ are acquired, the displacement gradient $\Delta\varepsilon$ is detected by each axial layer texture displacement of each plaque. The displacement gradient (strain) of each layer with a constant thickness of h_0 is obtained as follows:

$$\Delta\varepsilon(x, y, n) = (v(x + 1, y, n) - v(x, y, n))/h_0. \quad (1)$$

The maximum strain of each layer during one cardiac cycle is obtained by:

$$\Delta\varepsilon_{\max}(x, y) = \max_k |\Delta\varepsilon(x, y, n)| \quad (2)$$

Then the elastic modulus distribution is calculated. Phantom and animal plaques are assumed to be incompressible, the elastic modulus distribution is estimated by Hasegawa [46]:

$$E(x, y) = \frac{1}{2}\left(\frac{R_{il}}{h_0 \cdot M} + \frac{M - x + 1}{M}\right)\frac{\Delta P}{\Delta\varepsilon_{\max}(x, y)} \quad (3)$$

where M and R_{il} are the number of layers and the inner radius of the l-th layer, respectively, and ΔP is the pulse pressure difference. The layers indicate that the plaque has been divided n layers, and axial displacement is calculated each layer in the ROI region [44]. Here, h_0 is the thickness of the axial adjacent layer blood vessel wall in one cardiac cycle and $\Delta\varepsilon_{\max}$ is the largest displacement gradient for each layer in one cardiac cycle. The assumptions are that the isotropy and Poisson ratio are 0.5.

In previous studies, the axial strain or lateral strain calculated assumes that the entire vessel wall is homogeneous (only one value is calculated). However, the elastic modulus of each layer of tissue in the plaque is different. Our method potentially has the capacity for calculating the strain of each layer of tissue and then estimating the elastic modulus distribution.

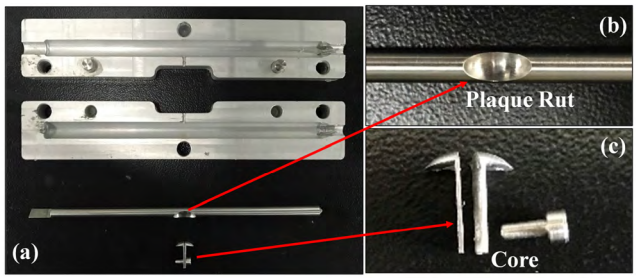

FIGURE 1. Photographs of metal shells, metal bars and metal caps used to construct vessel plaque phantoms: (a) One 12.6 mm hollow cuboid, 7.9 mm solid cylinders with a 50% stenosis groove and a mental mold; (b) Solid cylinders with a 50% stenosis rut; (c) Metal cap for formation of lipid core.

C. PHANTOM PREPARATION

Polyvinyl Alcohol Cryogel (PVA) (MW 146000–186000; 99+% hydrolysed, Sigma-Aldrich, USA) is widely applied to phantom experiment and is adopted to mimic vessel and plaque phantom [47]–[49]. In this study, a PVA phantom consists of 87% ultrapure water, 10% PVA powder and 3% cellulose powder (Type 20, Sigma-Aldrich, USA) three components. The production procedure is as follows: firstly, stir PVA powder in ultrapure water continually using a DF-101S magnetic stirrer (Gongyi Yuhua Instrument Co., Ltd., Gongyi, Heinan, China) at 20°C for 1.5 hour. Then, add the cellulose powder and the stir them at a 95°C for 1 hour. After that, the solution is cooled to 20°C and poured into a metal mould. As shown in Figure 1, the metal mould consists of a metal shell, a metal bar and a metal cap composed of two identical parts. Finally, the formation of the cryogel phantoms are induced by placing the model into a freezer and subjected to several repeated freeze-thaw cycles.

As a cryogel, the material obtains its rigidity via a freeze-thaw process and the stiffness of the material increases as the number of freeze-thaw cycles increase. Each cycle consists of two phases freezing at −20°C for 12 hours and thawing at 20°C for 12 hours. In Figure 2, all the samples experienced 1–8 freeze-thaw cycles, and elastic modulus of the phantoms are between 50 kPa–350 kPa.

Four different phantom sets were fabricated in this study: (1) Three phantoms with two components: soft tissue that underwent one freeze-thaw cycle PVA accounting for 10%, 40% and 64% of the total plaque volume, respectively, and surrounding tissue of the plaque phantom that underwent five freeze-thaw cycles. (2) A phantom with three components: soft tissue that underwent one freeze-thaw cycle and hard tissue that underwent three freeze-thaw cycles accounting for 32% respectively of the total plaque volume, the surrounding tissue of phantom plaque underwent eight freeze-thaw cycles

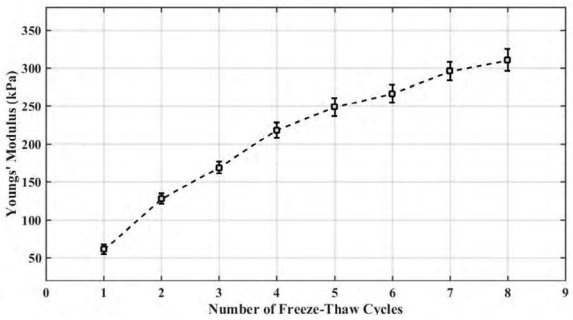

FIGURE 2. Elastic modulus of PVA phantoms in different numbers of freeze-thaw cycles measured by CMT-6104 electronic tensile tester.

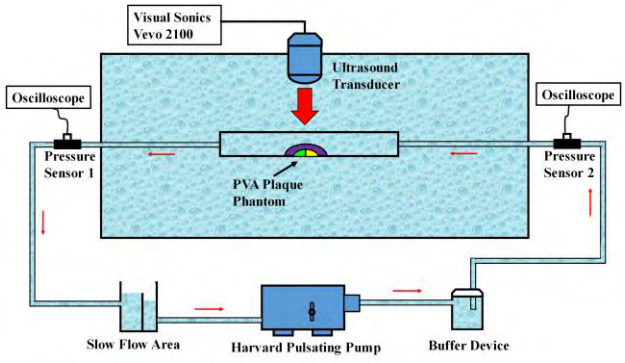

FIGURE 3. Experimental set-up simulated extracorporeal circulation was used to measure the elastic modulus distribution of *in vitro* plaque phantoms.

(plaque: length: 15 mm; degree of stenosis: 50%; phantom: wall thickness: 1 mm; inner radius: 5 mm; length: 100 mm).

D. PHANTOM TENSILE EXPERIMENT

The average elastic moduli of PVA cylindrical samples in different freeze-thaw cycles were verified by an electronic universal material testing machine (CMT-6104, New Sans Machinery Co., Ltd., Shenzhen, Guangdong, China). The methods are as follows: (1) measure the height and diameter of each sample by vernier caliper, mean values are obtained by five times; (2) obtain the force F exerted on the samples and height change ΔL of the samples by pressure sensor and displacement sensor. The elastic moduli are calculated by:

$$E = \frac{\sigma}{\varepsilon} = \frac{F/(\pi d^2)}{\Delta L/L} \tag{4}$$

where σ and ε are the stress and strain exerted on the samples, d and L are diameter and initial height of each samples.

Moreover, in Figure 2, all the samples experienced $1-8$ freeze-thaw cycles, and elastic modulus of the phantoms are between 50 kPa -350 kPa.

E. IN VITRO PLAQUE PHANTOMS EXPERIMENTS

The diagram of experimental system is shown in Figure 3. A pulsatile pump (Model 55-3305; Harvard Apparatus, Holliston, MA, USA) was used to mimic heart to provide power for human blood flow. The heart rate, pulsating flow and systolic-diastolic ratio were 45 beats min-1, 15L/stroke and 35/65, respectively. Systolic-diastolic ratio is the ratio of blood flow per minute during systolic and diastolic period. A buffer device was served as reducing the strong impact from pulsatile pump. A pressure transducer (HDP708, HeDi Sensor Instrument Co., Ltd., Foshan, Guangdong, China) connected with a digital oscilloscope (Teledyne LeCroy, Wavesurfer 3024, Chestnut Ridge, NY, USA) was installed between the buffer device and phantoms. The oscilloscope recorded the intraluminal pressure logged by the pressure transducer. The cine-loops of plaque were captured by MS550S transducer (transmit frequency: 40 MHz; frame rate: 117 Hz) and Vevo 2100 high resolution ultrasound imaging system (Vevo 2100, VisualSonics, Inc., Toronto, Canada). Two different ultrasound transducers are used in the paper because the depth of plaques are different in the *in vitro* and *in vivo* experiments. Note that B-mode images were acquired for a 4–5 s cine-loop and were decomposed into 350–450 frame images for each phantom. The focal depth was 6 mm and field of view was 15.5 mm (depth) by 10 mm (width). The size of interrogation window was 285 $\times$ 103 (pixels2) and the overlap was 55%. The cine-loop of each phantom was collected for three times. The area of different elastic modulus of soft tissue, hard tissue and surrounding tissue area calculated by the texture matching method were quantified by manual segmentation with the help from a doctor using ImageJ Software (64-bit, version 1.47v, National Institutes of Health, Bethesda, MD, USA). The percentage of these tissues calculated by the texture matching method were compared to the phantoms fabricated above.

F. IN ANIMAL EXPERIMENTS

The texture matching method was investigated with an in vivo preliminary study performed with six male ApoE knockout mice and three adult male New Zealand white rabbits. And all the mice (weight: about 40g) were fed a high-fat diet containing 21% lard and 0.15% cholesterol for a period of 5 to 20 weeks. After the plaques were found, the ultrasound experiment was performed about the 20th week and the mice were subsequently euthanized. Each rabbit model of an abdominal aortic plaque was established by under general anesthesia and underwent balloon-induced abdominal aortic endothelial damage. Following balloon-induced damage, both the rabbits were maintained on a high-fat diet (120–140 g/day of 1% cholesterol and 99% standard rabbit diet) for a period of 5 to 24 weeks. The ultrasound experiment was performed on about the 24th week and the rabbits were subsequently euthanized. All the mice (20 weeks) and rabbits (about 24 weeks) were raised in individual cages in Peking University Shenzhen Hospital. The protocol was approved by the institutional review board of Shenzhen Institutes of Advanced Technology, Chinese Academy of Sciences.Mice experiment procedures were as follows: firstly, the mice were anesthetized with Avertin, and then abdominal

regions were shaved. The B-mode movies of the abdominal aorta plaques were acquired over four cardiac cycles about 3–4s cine-loops were decomposed into 450–600 B-mode images, using a MS250 linear array transducer (transmit frequency: 20 MHz; frame rate: 100 Hz). The focus depth range was 2–3 mm depending on the individual differences. Blood pressure was referred to the standard value of mice blood pressure. In this study, a final 139×30 (pixels^2) interrogation window with an overlap ratio of 50% was used.

The rabbit experiment steps were as follows: firstly, rabbits were anesthetized with an intravenous injection of 3% Phenobarbital and fixed on the inspection table, then the abdominal areas were shaved. Next, the B-mode movies of the abdominal aorta plaques were acquired over four cardiac cycles about 3–4s cine-loop and 350–450 B-mode images, using a MS250 linear array transducer (transmit frequency: 20 MHz; frame rate: 100 Hz). The focus depth range was 5–5.5 mm depending on the individual differences. Blood pressure was referred to the standard value of rabbit blood pressure. In this study, a final 278×58 (pixels^2) interrogation window with an overlap ratio of 55% was used in texture matching analysis.

Vulnerability-Index (VI) was used to evaluate the overall degree of vulnerability [50], [51]. VI was calculated by the relation between analyzed unstable (U) and stable (S) features of the plaques. The formula for VI was expressed as $VI_i = U_i/V_i$, where U includes unstable region, the lipid region area, and V includes stable region, the sum of fiber tissue and calcification area in the study, where i represents each mouse and rabbit.

All data were calculated three times and expressed as mean ± SD. Statistical significance was performed by paired-samples t-test, which were conducted using SPSS statistics (Version 20, IBM Corporation, Chicago, IL, USA). Statistical power $(1-\beta)$ were performed by G*Power 3 (Version 3.1.9.4, Germany). Because of the small size *in vivo* experiment, statistical significance was performed by paired-samples t-test between elastography and histography.

Initially, ten ApoE knockout mice and five adult male New Zealand white rabbits were raised for the experiment. Because the integrated plaque tissue was hard to acquire, five mice and two rabbits expired in the process of animal raising. Also, the plaques did not form in six mice and five rabbits. Consequently, only six results from mice and three results from rabbits were adopted. Mouse and rabbit husbandry and all the procedures used in the study were performed in accordance with the guidelines and regulations of the Shenzhen Institutes of Advanced Technology, Chinese Academy of Sciences.

G. HISTOLOGY

The histology method of mice and rabbit is identical and the procedures are as follows: After the mice and rabbits were euthanized, the plaques were collected and were snap-frozen. A series of frozen sections (20 μm) were obtained for histological examination. The frozen sections were acquired at 1 mm on either side of the maximum longitudinal section and were utilized for hematoxylin and eosin (G1005, Servicebio, Wuhan, Hubei, China), Masson (G1006, Servicebio, Wuhan, Hubei, China), Oil Red O (G1016, Servicebio, Wuhan, Hubei, China) and Von Kossa (G1016, Servicebio, Wuhan, Hubei, China) staining, which identified fibrous tissue (blue), lipid area (red), as well as calcification (black). Stained images were scanned and showed by CaseViewer software (3DHISTECH, Budapest, Hungary).

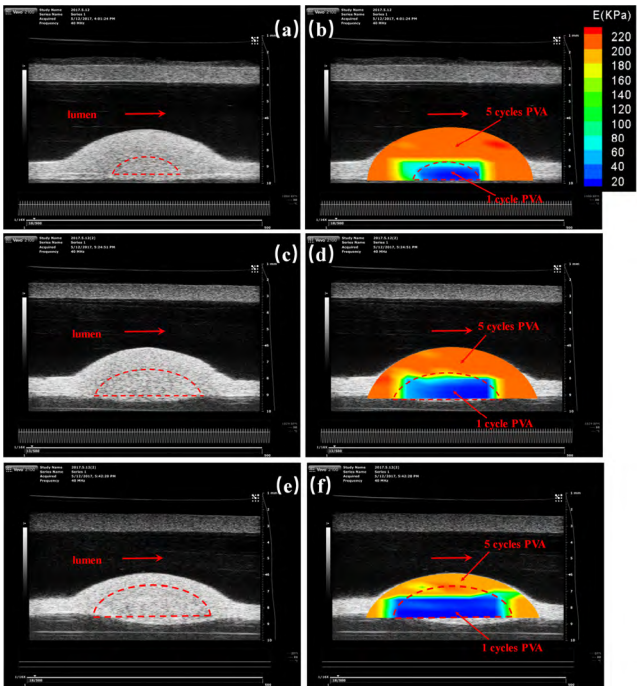

FIGURE 4. Ultrasound images and elastic distribution image of plaque phantoms of two components calculated by texture matching method: (a), (c) and (e) is B-mode images of soft tissue accounts for 10%, 40% and 64% of the total plaque volume, respectively; (b), (d) and (f) shows elastic distribution of the three different percentage plaque phantoms.

III. RESULTS

A. TWO COMPONENT PHANTOM EXPERIMENT

Figure 4 indicates the elastic modulus distribution of soft tissue respectively accounted for 10% (a), 40% (c) and 64% (e) of the total plaque volume of two component phantom plaques. It shows that the soft tissue (red region) embedded in the plaque can be clearly distinguished from surrounding tissues (blue region) by the elastic distribution. Additionally, the mean elastic modulus of the soft tissue is significantly lower than the elastic modulus within the surrounding tissue. The mean elastic moduli of three experiments in soft tissue are 43.7 ± 5.5 kPa, 67.2 ± 10.5 kPa and 58.2 ± 7.8 kPa, respectively, while the mean elastic moduli of surrounding regions are 195.0 ± 16 kPa, 199.8 ± 7.7 kPa and 200.5 ± 7.7 kPa, respectively. The mean elastic moduli are also compared to the experimental value verified on the electronic universal material testing machine in Figure 3. The mean elastic modulus of soft tissue subjected one freeze-thaw cycle

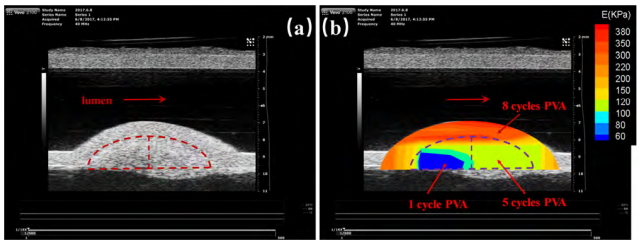

FIGURE 5. Ultrasound images and elastic distribution image of plaque phantoms of three components calculated by texture matching method: (a) B-mode images of soft tissue and hard tissue accounts for 32% respectively of the total plaque volume; (b) shows elastic distribution of the plaque phantom.

is 60.9 ± 6.8 kPa, and the mean elastic modulus of stiff tissue experienced five freeze-thaw cycles is 248.8 ± 12.1 kPa. In comparison, a difference of 5.1% and 20.3% are compared between calculated mean values by the texture matching method and experimental value by tensile experiment in one and five freeze-thaw cycles. A three-component phantom is also measured by the texture matching method as shown in Figure 5. Three regions respectively experienced one, five and eight freeze-thaw cycles and the mean elastic modulus of eight freeze-thaw cycles is 381.6 ± 3.8 kPa calculated by texture matching method and mean elastic modulus of PVA subjected eight freeze-thaw cycles is 310.3 ± 14.1 kPa tested by the experiment. A difference of 23.0% is compared by the electronic universal material testing machine again.

B. ANIMAL EXPERIMENT

In order to ensure the reliability of the experimental results, only large and intact plaques were adopted as follows: six abdominal aortic plaque of mice (Plaque1, Plaque2, Plaque3, Plaque4, Plaque5 and Plaque6) and three abdominal aortic plaque of rabbits (Plaque1, Plaque2 and Plaque3) are evaluated in this section.

Figure 6 (a) shows an example of a plaque (height: 0.6 mm, length: 3.9 mm) containing heterogeneous tissue in one abdominal aorta of a mouse. Based on the B-mode image, the plaque contains low echo intensity in the right region and high echo intensity in the left region. The elastic distribution of the plaque calculated by the texture matching method is displayed in Figure 6 (b). It shows that the elastic modulus of the tissue in the right region is apparently higher than the left. Figure 6 (c) shows hematoxylin and eosin histological staining that displays the morphological characteristic of the plaque and the outline of the plaque labeled by green line. Figure 6 (d) demonstrates Masson histological staining with a mass of dark blue region, which identifies the presence of collagen in the fibrous tissue. Figure 6 (e) shows Oil Red O staining, and red area is showed on the right side of the plaque that demonstrates the existence of lipid tissue. Figure 6 (f) shows that the plaque is absence of calcification verified by Von Kossa staining. The soft region and stiff regions and lipid tissue and calcification are quantified by ImageJ software, respectively and the percentage are showed

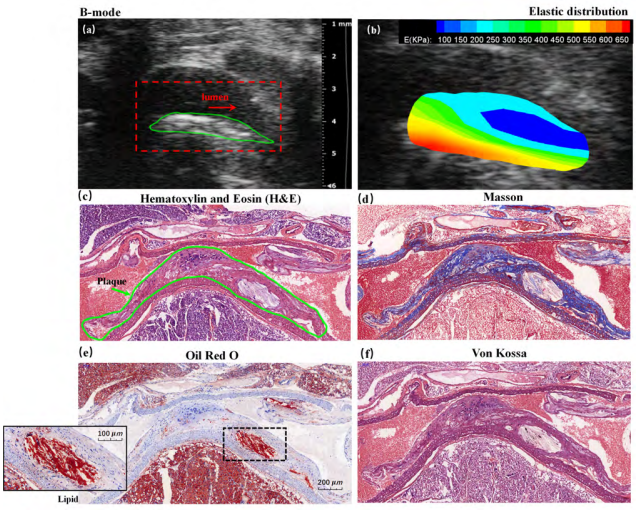

FIGURE 6. Texture matching method based on B-mode calculates elastic distribution of a mouse abdominal aorta plaque: (a) shows B-mode image of the plaque; (b) shows the image of elastic distribution and identifies the presence of lipid (blue) and fibrous tissue (yellow and green). These plaque components are confirmed by Hematoxylin and Eosin (H&E) (c) and Masson (d) and Oil Red O (e) staining on histology on adjacent frozen section.

in Table 1. Plaque 1 (the plaque in Figure 6) shows that lipid and calcification regions occupy 5.00 ± 0.44% and 5.76 ± 0.35% via elastography. Plaque 2 shows that the lipid and calcification regions occupy 34.34 ± 1.52% and 3.04 ± 0.44% via elastography, and 34.18 ± 0.56% and 4.30 ± 0.05% via histology. The percentage of lipid tissue and calcification calculated in plaque 1 and plaque 2 in Table 1 are in good agreement with histological examination. Similarly, other plaques (plaque 3, plaque 4, plaque 5, plaque 6) from mice also show great agreement in elastography and histological examination (lipid: $n = 6, p = 0.987$, power $(1 - \beta) = 0.887$). The VI of plaques of all mice have been calculated and supplemented in Table 1. Apparently, plaque 2 and plaque 3 contained more lipid region means high vulnerability.

Figure 7 shows a rabbit example of composited components of abdominal aortic plaque. Figure 7 (a) shows the B-mode image of the plaque contained partial calcification (height: 1.8 mm, length: 3.0 mm). Figure 7 (b) displays the elastic distribution of the plaque. In comparison, figure 8 (c) shows morphology of the plaque stained by Hematoxylin and Eosin. Figure 7 (d) demonstrates mazarine region on the left of the plaque stained by Masson, which means fiber tissue is rich in this case. Figure 7 (e) shows Oil Red O histological stainingof the plaque, showing the existence of some lipid tissue. Finally, on the tight side of the Von Kossa staining, the black religion demonstrates the existence of calcification. The position and the characteristics of plaque calculated by the texture method are in significant agreement with the histological examination. The percentages of lipid tissue, fiber tissue and calcification are showed in Table 2. Plaque 2 in Table 2 (the plaque in Figure 7) shows that

TABLE 1. The percentage of lipid tissue and calcification of elastography and histology in mice plaques.

		Lipid tissue (%)	Calcification (%)	Vulnerability-Index (VI)
Plaque1	Elastography	5.00 ± 0.44	0.00	0.064 ± 0.004
	Histology	5.76 ± 0.35	0.00	0.069 ± 0.004
Plaque2	Elastography	34.34 ± 1.52	3.04 ± 0.44	0.597 ± 0.036
	Histology	34.18 ± 0.56	4.30 ± 0.05	0.600 ± 0.003
Plaque3	Elastography	27.62 ± 0.63	0.00	0.432 ± 0.012
	Histology	23.59 ± 0.35	0.00	0.356 ± 0.023
Plaque4	Elastography	7.03 ± 0.54	0.00	0.110 ± 0.003
	Histology	8.95 ± 0.18	0.00	0.090 ± 0.004
Plaque5	Elastography	11.35 ± 0.85	0.00	0.124 ± 0.015
	Histology	15.76 ± 1.43	0.00	0.197 ± 0.016
Plaque6	Elastography	14.38 ± 1.31	4.80 ± 0.47	0.048 ± 0.005
	Histology	11.70 ± 0.35	5.04 ± 0.34	0.050 ± 0.003

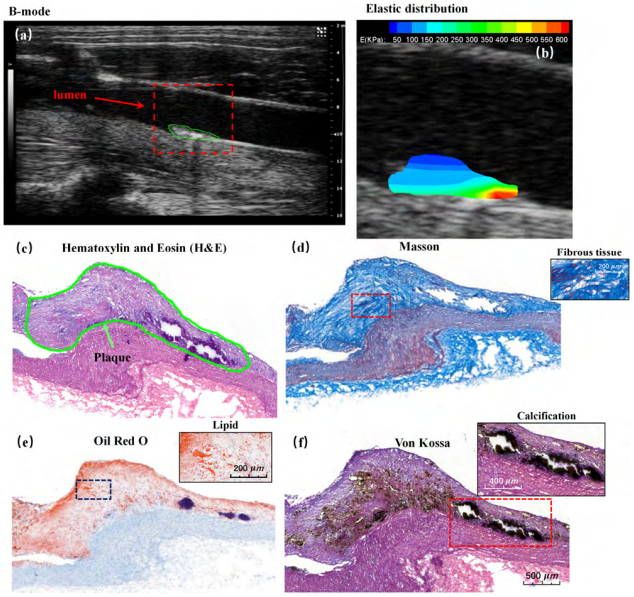

FIGURE 7. Texture matching method based on B-mode calculates elastic distribution of another rabbit abdominal aorta plaque: (a) shows B-mode image of the plaque; (b) shows the image of elastic distribution and identifies the presence of lipid (blue), fibrous tissue (yellow and green) and calcium (red). These plaque components are confirmed by Hematoxylin and Eosin (H&E) (c), Masson (d), Oil Red O (e) and Von Kossa's staining on histology on adjacent frozen section.

lipid and calcification region occupy 20.05 ± 1.90% and 7.51 ± 0.56% via elastography, and 15.56 ± 1.40% and 10.44 ± 0.72% via histology. The percentage of lipid tissue and calcification calculated from all the plaques from rabbits are in good agreement with histological examination. Similarly, other plaques (plaque 1 and plaque 3) from rabbits also show great agreement in elastography and histological examination in Table 2 (lipid: $n = 3$, $p = 0.077$, power $(1 - \beta) = 0.697$). The VI value of plaques of all rabbits have been calculated and supplemented in Table 2. Apparently,

TABLE 2. The percentage of lipid tissue and calcification of elastography and histology in rabbit plaques.

		Lipid tissue (%)	Calcification (%)	Vulnerability-Index (VI)
Plaque1	Elastography	43.82 ± 1.33	0.00	1.057 ± 0.025
	Histology	42.52 ± 1.54	0.00	1.325 ± 0.077
Plaque2	Elastography	19.47 ± 1.95	7.51 ± 0.56	0.387 ± 0.038
	Histology	16.95 ± 0.85	10.44 ± 0.72	0.562 ± 0.052
Plaque3	Elastography	39.34 ± 1.87	0.00	0.802 ± 0.039
	Histology	38.37 ± 3.00	0.00	0.723 ± 0.057

plaque 1 and plaque 3 contained more lipid region means high vulnerability.

IV. DISCUSSION

The composition of atherosclerotic plaque is a significant marker of the vulnerability of plaques [52], [53]. We propose a texture matching method to distinguish plaques with two and three components in phantom study. Further, the effectiveness of the method for evaluating elastic moduli distribution of animal plaques is validated by histological staining. The results demonstrate the potential of the texture matching method in estimating the elastic distribution of the plaques, which is promising in assessing the vulnerability of the atherosclerotic plaque and predicting the risk of cardiovascular disease.

The soft tissue area of elastography of plaque phantoms calculated by texture matching method was also quantified by an ImageJ Software. The percentage of area of one cycle region are 12.3%, 36.7% and 58.7% calculated by texture matching method, which are existed 2.3%, 3.3% and 5.3% difference with 3 phantom plaques, respectively. Furthermore, in the three components phantom, the percentage of area of one cycle and five cycles region were 26.4% and 27.7% percentage of the whole phantom plaque calculated by texture matching method, in comparison, and existed 5.6% and 4.3% difference with the phantom plaque. The cause of the deviation may be determined by problem of the experimental system, for example, the sealing of the experimental system may all result in some experimental errors. All of the factors could be related to low accuracy of the method. Moreover, selection of diagnostic window plays an important role in the accuracy and reliability of elastic modulus calculations in two consecutive B-mode images. If the diagnostic window is not large enough, it is difficult to implement the method because of insufficient plaque texture information in ROI. On the contrary, if the diagnostic window is too large, the spatial resolution will be affected. Normally, the selection of the interrogation window follows the 'one-quarter rule' provided by Adrian [54], which means that the displacement of texture must less than or equal to one quarter the size of the interrogation window. In Figure 5-7, the boundary of the plaques looks uniform, sharp and clear, and it is because the sub-pixel method, the Gaussian peak filter and

interpolation method are utilized in the acquisition of the elastic distribution.

The range of estimated elastic modulus *in vitro* experiment varies from 50 kPa to 350 kPa approximately, which is tested by the phantom tensile experiment (see Figure 2). This scope is basically consistent with the elasticity of biological tissues. Elastic moduli have been reported to vary in such a range for human tissues, especially for undiseased tissue, common carotid artery [55]. Further, the average elastic moduli of PVA phantoms in different freeze-thaw cycles were compared other identical materials studied in phantom experiment. Ramnarine *et al.* have found the mean elastic modulus of PVA phantoms subjected to two and five freeze-thaw cycles were 43 kPa and 170 kPa, respectively [40]. The elastic modulus is basically consistent with 56.4 kPa and 198.4 kPa calculated by our method (see Figure 3). While in Fromageau *et al.* study, PVA phantoms were 25 ± 3.0 kPa, 302 ± 35 kPa and 465 ± 53 kPa in one, five and eight freeze-thaw cycles measured by tensile experiment [56], were a slightly higher than our results. The different elastic modulus of PVA phantoms probably caused by the concentration of acoustic scatterer, the temperature and humidity of the freeze-thaw process and different algorithms.

In vivo study, only soft tissue and hard tissue components were distinguishable via the texture matching method. Lipid and fiber tissue were evaluated by histological verification, but intraplaque hemorrhage (IPH) and vasa vasorum in plaques could not be observed by our method. Notably, vasa vasorum is of significance as an indicator of vulnerability of plaque [57]. Further, the thickness of the fibrous cap was also referred to estimate the vulnerability of the plaque [52], whereas it was difficult to identify the specific thickness of fibrous cap by our method due to the resolution. The problem may possibly be resolved by acquiring a B-mode image of high resolution and applying a smaller interrogation window in the future. So, the method might be utilized in clinical ultrasound equipment to detect atherosclerotic disease in the near future.

We have also compared to previous methods, like ultrasound radiofrequency (RF) data and RF signal envelope data was used to estimate strain of plaques, while it was hard to acquire clinical data of raw clinical data and the quantity of the data of one case was too large, wasting a lot of processing time [37], [38]. Shear wave elastography was a common measure to quantify elastic modulus distribution in atherosclerotic plaque. However, the pulsation of the vessel wall is a limitation affecting the accuracy of the SWE and the method also based on assumptions of linear behavior in an isotropic, semi-infinite medium. Therefore, the method based by B-mode data is a more appropriate choice.

V. LIMITATIONS OF THE STUDY

Our study also has some limitations that exist in the experiment and need to be addressed in the future. Firstly, the plaque phantoms cannot be fabricated the same size as the real plaque because of the characteristics and difficulties of the plaque fabrication process. Besides, the frame rate (at least 80 Hz) of the ultrasound equipment is a key parameter in the experiment, because this parameter directly affects the feasibility of the cross-correlation algorithm. At present, most ultrasound imaging systems for small animals, even clinical equipment can provide higher frame rates. And eliminating the tissue motion is also an issue. In the experiment, all animals were anesthetized and maintained breathing while capturing the B-mode data to eliminate the affect of motion. Another limitation is that the elastic moduli of animal plaques *in vivo* cannot be calculated and verified. However, the absolute elastic modulus is not so crucial for the stiffness distribution and it is sufficient to determine in affirming the presence and percentage of lipid tissue. In addition, the blood pressure of rabbits is estimated by referring to the normal value. Moreover, we do not measure the blood pressure from mice and rabbits and the open question is to further verify our texture matching method by clinical experiment. Pressure guide wire can be a method to measure pressure in animal organs. In addition, in a clinical scenario, brachial artery pressure can be readily measured. The absolute values are not acquired from the *in vivo* experiment. The elastography combined with echo intensity is a reliable means for identifying the components of the plaque and the absolute values from the *in vivo* experiment can be the focus of future. Manually segmenting the plaque in ultrasound images is prone to deviation and in our experiment, the plaque profiles were extracted by a specialized physician. Animal modeling is also a limitation. Atherosclerosis may cause myocardial infarction, cerebral infarction and cerebral hemorrhage, leading to high mortality in the rabbit and mouse models. The animal validation study is relatively small, and the number of animal experiments and clinical experiments should be increased in the future.

VI. CONCLUSION

In conclusion, the study provided phantom verification and histological validation of the texture matching method for differentiating soft and stiff plaque tissues. The method quantified elastic modulus distribution to assess the vulnerability of the plaque. This technique may be of value in patients to prevent of the occurrence of stroke and other cardiovascular diseases and evaluate the effect of drug treatment for vulnerable plaque in a clinical setting.

ACKNOWLEDGMENT

(Hongyu Kang and Yanling Zhang are co-first authors.)

REFERENCES

[1] E. J. Benjamin, "Heart disease and stroke statistics-2017 update: A report from the American heart association," *Circulation*, vol. 135, no. 10, pp. e146–e603, 2017.

[2] A. V. Finn, M. Nakano, J. Narula, F. D. Kolodgie, and R. Virmani, "Concept of vulnerable/unstable plaque," *Arterioscler Thromb Vascular Biol.*, vol. 30, no. 7, pp. 1282–1292, Jul. 2010, doi: 10.1161/ATVBAHA.108.179739.

[3] M. Naghavi, "From vulnerable plaque to vulnerable patient: A call for new definitions and risk assessment strategies: Part II," *Circulation*, vol. 108, no. 15, pp. 1772–1778, Oct. 2003, doi: 10.1161/01.CIR.0000087481.55887.C9.

[4] R. Virmani, A. P. Burke, A. Farb, and F. D. Kolodgie, "Pathology of the vulnerable plaque," *J. Amer. College Cardiol.*, vol. 47, no. 8, p. C13, 2006.
[5] M. C. Fishbein, "The vulnerable and unstable atherosclerotic plaque," *Cardiovascular Pathol.*, vol. 19, no. 1, pp. 6–11, Jan./Feb. 2010, doi: 10.1016/j.carpath.2008.08.004.
[6] R. Waksman, R. Torguson, M.-A. Spad, H. Garcia-Garcia, J. Ware, R. Wang, S. Madden, P. Shah, and J. Muller, "The lipid-rich plaque study of vulnerable plaques and vulnerable patients: Study design and rationale," *Amer. Heart J.*, vol. 192, pp. 98–104, Oct. 2017.
[7] S. E. Nissen, "Clinical images from intravascular ultrasound: Coronary disease, plaque rupture, and intervention–the inside view," *Amer. J. Cardiol.*, vol. 88, no. 8, pp. 16–18, Oct. 2001.
[8] J. A. Schaar, "Characterizing vulnerable plaque features with intravascular elastography," *Circulation*, vol. 108, no. 21, pp. 2636–2641, Nov. 2003, doi: 10.1161/01.CIR.0000097067.96619.1F.
[9] S. Le Floc'h, G. Cloutier, G. Finet, P. Tracqui, R. I. Pettigrew, and J. Ohayon, "On the potential of a new ivus elasticity modulus imaging approach for detecting vulnerable atherosclerotic coronary plaques: *In vitro* vessel phantom study," *Phys. Med. Biol.*, vol. 55, no. 19, pp. 5701–5721, Oct. 2010, doi: 10.1088/0031-9155/55/19/006.
[10] M. S. Richards, R. Perucchio, and M. M. Doyley, "Visualizing the stress distribution within vascular tissues using intravascular ultrasound elastography: A preliminary investigation," *Ultrasound Med. Biol.*, vol. 41, no. 6, pp. 1616–1631, Jun. 2015, doi: 10.1016/j.ultrasmedbio.2015.01.022.
[11] X. B. Hu, "Intravascular ultrasound area strain imaging used to characterize tissue components and assess vulnerability of atherosclerotic plaques in a rabbit model," *Ultrasound Med. Biol.*, vol. 37, no. 10, pp. 1579–1587, Oct. 2011, doi: 10.1016/j.ultrasmedbio.2011.06.025.
[12] Z. Li, L. Wang, X. Hu, P. Zhang, Y. Chen, X. Liu, M. Xu, Y. Zhang, and M. Zhang, "Effect of rosuvastatin on atherosclerotic plaque stability: An intravascular ultrasound elastography study," *Atherosclerosis*, vol. 248, pp. 27–35, May 2016, doi: 10.1016/j.atherosclerosis.2016.02.028.
[13] Y. Majdouline, J. Ohayon, Z. Keshavarz-Motamed, M.-H. Roy Cardinal, D. Garcia, L. Allard, S. Lerouge, F. Arsenault, G. Soulez, and G. Cloutier, "Endovascular shear strain elastography for the detection and characterization of the severity of atherosclerotic plaques: *In vitro* validation and *in vivo* evaluation," *Ultrasound Med. Biol.*, vol. 40, no. 5, pp. 890–903, May 2014.
[14] G. A. Rodriguez-Granillo, "*In vivo* intravascular ultrasound-derived thin-cap fibroatheroma detection using ultrasound radiofrequency data analysis," *J. Amer. College Cardiol.*, vol. 46, no. 11, pp. 2038–2042, Dec. 2005, doi: 10.1016/j.jacc.2005.07.064.
[15] G. A. Rodriguez-Granillo, "Coronary artery remodelling is related to plaque composition," *Heart*, vol. 92, no. 3, pp. 388–391, Oct. 2005.
[16] A. J. Brown, D. R. Obaid, C. Costopoulos, R. A. Parker, P. A. Calvert, Z. Teng, S. P. Hoole, N. E. J. West, M. Goddard, and M. R. Bennett, "Direct comparison of virtual-histology intravascular ultrasound and optical coherence tomography imaging for identification of thin-cap fibroatheroma," *Circulat. Cardiovascular Imag.*, vol. 8, no. 10, Oct. 2015, Art. no. e003487, doi: 10.1161/CIRCIMAGING.115.003487.
[17] E. B. Diethrich, M. P. Margolis, D. B. Reid, A. Burke, V. Ramaiah, J. A. Rodriguez-Lopez, G. Wheatley, D. Olsen, and R. Virmani, "Virtual histology intravascular ultrasound assessment of carotid artery disease: The carotid artery plaque virtual histology evaluation (CAPITAL) study," *J. Endovascular Therapy*, vol. 14, no. 5, pp. 676–686, Oct. 2007.
[18] R. De Rosa, M. Vasa-Nicotera, D. M. Leistner, S. M. Reis, C. E. Thome, J.-N. Boeckel, S. Fichtlscherer, and A. M. Zeiher, "Coronary atherosclerotic plaque characteristics and cardiovascular risk factors—Insights from an optical coherence tomography study," *Circulat. J.*, vol. 81, no. 8, pp. 1165–1173, 2017, doi: 10.1253/circj.CJ-17-0054.
[19] G. J. Tearney *et al.*, "Consensus standards for acquisition, measurement, and reporting of intravascular optical coherence tomography studies," *J. Amer. College Cardiol.*, vol. 59, no. 12, pp. 1058–1072, 2012.
[20] Y. Miyamoto, "Plaque characteristics of thin-cap fibroatheroma evaluated by OCT and IVUS," *Cardiovascular Imag.*, vol. 4, no. 6, pp. 638–646, Jun. 2011, doi: 10.1016/j.jcmg.2011.03.014.
[21] J. Hou, "Comparison of intensive versus moderate lipid-lowering therapy on fibrous cap and atheroma volume of coronary lipid-rich plaque using serial optical coherence tomography and intravascular ultrasound imaging," *Amer. J. Cardiol.*, vol. 117, no. 5, pp. 800–806, Mar. 2016, doi: 10.1016/j.amjcard.2015.11.062.
[22] G. Niccoli, "Plaque rupture and intact fibrous cap assessed by optical coherence tomography portend different outcomes in patients with acute coronary syndrome," *Eur. Heart J.*, vol. 36, no. 22, pp. 1377–1384, Jun. 2015, doi: 10.1093/eurheartj/ehv029.
[23] S. Rathore, "Association of coronary plaque composition and arterial remodelling: A optical coherence tomography study," *Atherosclerosis*, vol. 221, no. 2, pp. 405–415, Apr. 2012, doi: 10.1016/j.atherosclerosis.2011.10.018.
[24] G. van Soest, "Pitfalls in plaque characterization by OCT: Image artifacts in native coronary arteries," *Cardiovascular Imag.*, vol. 4, no. 7, pp. 810–813, Jul. 2011, doi: 10.1016/j.jcmg.2011.01.022.
[25] S. A. Kruse, "Magnetic resonance elastography of the brain," *NeuroImage*, vol. 39, no. 1, pp. 231–237, Jan. 2008, doi: 10.1016/j.neuroimage.2007.08.030.
[26] A. Manduca, T. E. Oliphant, M. A. Dresner, J. L. Mahowald, S. A. Kruse, E. Amromin, J. P. Felmlee, J. F. Greenleaf, and R. L. Ehman, "Magnetic resonance elastography: Non-invasive mapping of tissue elasticity," *Med. Image Anal.*, vol. 5, no. 4, pp. 237–254, Dec. 2001.
[27] Y. K. Mariappan, K. J. Glaser, and R. L. Ehman, "Magnetic resonance elastography: A review," *Clin. Anatomy*, vol. 23, no. 5, pp. 497–511, Jun. 2010, doi: 10.1002/ca.21006.
[28] D. B. Plewes, J. Bishop, A. Samani, and J. Sciarretta, "Visualization and quantification of breast cancer biomechanical properties with magnetic resonance elastography," *Phys. Med. Biol.*, vol. 45, no. 6, pp. 1591–1610, Jun. 2000.
[29] T. Saam, "Quantitative evaluation of carotid plaque composition by *in vivo* MRI," *Arteriosclerosis, Thrombosis, Vascular Biol.*, vol. 25, no. 1, pp. 234–239, Jan. 2005, doi: 10.1161/01.ATV.0000149867.61851.31.
[30] Q. J. van den Bouwhuijsen, M. W. Vernooij, A. Hofman, G. P. Krestin, A. van der Lugt, and J. C. Witteman, "Determinants of magnetic resonance imaging detected carotid plaque components: The rotterdam study," *Eur. Heart J.*, vol. 33, no. 2, pp. 221–229, Jan. 2012, doi: 10.1093/eurheartj/ehr227.
[31] J. T. Chai, L. Biasiolli, L. Li, M. Alkhalil, F. Galassi, C. Darby, A. W. Halliday, L. Hands, T. Magee, J. Perkins, E. Sideso, A. Handa, P. Jezzard, M. D. Robson, and R. P. Choudhury, "Quantification of lipid-rich core in carotid atherosclerosis using magnetic resonance T_2 mapping," *Cardiovascular Imag.*, vol. 10, no. 7, pp. 747–756, Jul. 2017, doi: 10.1016/j.jcmg.2016.06.013.
[32] J. H. F. Rudd, E. A. Warburton, T. D. Fryer, H. A. Jones, J. C. Clark, N. Antoun, P. Johnstrom, A. P. Davenport, P. J. Kirkpatrick, B. N. Arch, J. D. Pickard, and P. L. Weissberg, "Imaging atherosclerotic plaque inflammation with [^{18}F]-fluorodeoxyglucose positron emission tomography," *Circulation*, vol. 105, no. 23, pp. 2708–2711, Jun. 2002, doi: 10.1161/01.cir.0000020548.60110.76.
[33] G. Delso, A. Martinez-Moller, R. A. Bundschuh, S. G. Nekolla, S. I. Ziegler, and M. Schwaiger, "Preliminary study of the detectability of coronary plaque with pet," *Phys. Med. Biol.*, vol. 56, no. 7, pp. 2145–2160, Apr. 2011, doi: 10.1088/0031-9155/56/7/016.
[34] H. Shi and T. Varghese, "Two-dimensional multi-level strain estimation for discontinuous tissue," *Phys. Med. Biol.*, vol. 52, no. 2, pp. 389–401, Jan. 2007, doi: 10.1088/0031-9155/52/2/006.
[35] C. Schmitt, G. Soulez, R. L. Maurice, M. F. Giroux, and G. Cloutier, "Noninvasive vascular elastography: Toward a complementary characterization tool of atherosclerosis in carotid arteries," *Ultrasound Med. Biol.*, vol. 33, no. 12, pp. 1841–1858, Dec. 2007, doi: 10.1016/j.ultrasmedbio.2007.05.020.
[36] H. H. G. Hansen, G. J. de Borst, M. L. Bots, F. L. Moll, G. Pasterkamp, and C. L. de Korte, "Validation of noninvasive *in vivo* compound ultrasound strain imaging using histologic plaque vulnerability features," *Stroke*, vol. 47, no. 11, pp. 2770–2775, Nov. 2016, doi: 10.1161/STROKEAHA.116.014139.
[37] M.-H. R. Cardinal, M. H. G. Heusinkveld, Z. Qin, R. G. P. Lopata, C. Naim, G. Soulez, and G. Cloutier, "Carotid artery plaque vulnerability assessment using noninvasive ultrasound elastography: Validation with MRI," *Amer. J. Roentgenol.*, vol. 209, no. 1, pp. 142–151, Jul. 2017, doi: 10.2214/AJR.16.17176.
[38] H. Kanai, H. Hasegawa, M. Ichiki, F. Tezuka, and Y. Koiwa, "Elasticity imaging of atheroma with transcutaneous ultrasound: Preliminary study," *Circulation*, vol. 107, no. 24, pp. 3018–3021, Jun. 2003, doi: 10.1161/01.CIR.0000078633.31922.8A.
[39] E. Widman, K. Caidahl, B. Heyde, J. D'hooge, and M. Larsson, "Ultrasound speckle tracking strain estimation of *in vivo* carotid artery plaque with *in vitro* sonomicrometry validation," *Ultrasound Med. Biol.*, vol. 41, no. 1, pp. 77–88, Jan. 2015, doi: 10.1016/j.ultrasmedbio.2014.06.013.

[40] K. V. Ramnarine, J. W. Garrard, K. Dexter, S. Nduwayo, R. B. Panerai, and T. G. Robinson, "Shear wave elastography assessment of carotid plaque stiffness: *In vitro* reproducibility study," *Ultrasound Med. Biol.*, vol. 40, no. 1, pp. 200–209, Jan. 2014, doi: 10.1016/j.ultrasmedbio.2013.09.014.

[41] J. J. Dahl, D. M. Dumont, J. D. Allen, E. M. Miller, and G. E. Trahey, "Acoustic radiation force impulse imaging for noninvasive characterization of carotid artery atherosclerotic plaques: A feasibility study," *Ultrasound Med. Biol.*, vol. 35, no. 5, pp. 707–716, May 2009, doi: 10.1016/j.ultrasmedbio.2008.11.001.

[42] T. J. Czernuszewicz, "Non-invasive *in vivo* characterization of human carotid plaques with acoustic radiation force impulse ultrasound: Comparison with histology after endarterectomy," *Ultrasound Med. Biol.*, vol. 41, no. 3, pp. 685–697, Mar. 2015, doi: 10.1016/j.ultrasmedbio.2014.09.016.

[43] E. Widman, E. Maksuti, D. Larsson, M. W. Urban, A. Bjallmark, and M. Larsson, "Shear wave elastography plaque characterization with mechanical testing validation: A phantom study," *Phys. Med. Biol.*, vol. 60, no. 8, pp. 3151–3174, Apr. 2015, doi: 10.1088/0031-9155/60/8/3151.

[44] L. Niu, M. Qian, R. Song, L. Meng, X. Liu, and H. Zheng, "A texture matching method considering geometric transformations in noninvasive ultrasonic measurement of arterial elasticity," *Ultrasound Med. Biol.*, vol. 38, no. 3, pp. 524–533, Mar. 2012, doi: 10.1016/j.ultrasmedbio.2011.12.010.

[45] L. Niu, "Ultrasonic particle image velocimetry for improved flow gradient imaging: Algorithms, methodology and validation," *Phys. Med. Biol.*, vol. 55, no. 7, pp. 2103–2120, Apr. 2010, doi: 10.1088/0031-9155/55/7/020.

[46] H. Hasegawa, H. Kanai, N. Hoshimiya, and Y. Koiwa, "Evaluating the regional elastic modulus of a cylindrical shell with nonuniform wall thickness," *J. Med. Ultrason.*, vol. 31, no. 2, pp. 81–90, Jun. 2004, doi: 10.1007/s10396-004-0014-y.

[47] S. Cournane, L. Cannon, J. E. Browne, and A. J. Fagan, "Assessment of the accuracy of an ultrasound elastography liver scanning system using a PVA-cryogel phantom with optimal acoustic and mechanical properties," *Phys. Med. Biol.*, vol. 55, no. 19, pp. 5965–5983, Oct. 2010.

[48] D. M. King, C. M. Moran, J. D. McNamara, A. J. Fagan, and J. E. Browne, "Development of a vessel-mimicking material for use in anatomically realistic Doppler flow phantoms," *Ultrasound Med. Biol.*, vol. 37, no. 5, pp. 813–826, May 2011.

[49] K. J. M. Surry, H. J. B. Austin, A. Fenster, and T. M. Peters, "Poly(vinyl alcohol) cryogel phantoms for use in ultrasound and MR imaging," *Phys. Med. Biol.*, vol. 49, no. 24, pp. 5529–5546, Dec. 2004.

[50] M. Shiomi, "Fibromuscular cap composition is important for the stability of established atherosclerotic plaques in mature WHHL rabbits treated with statins," *Atherosclerosis*, vol. 157, no. 1, pp. 75–84, Jul. 2001.

[51] H. Hartwig, C. Silvestre-Roig, J. Hendrikse, L. Beckers, N. Paulin, K. Van der Heiden, Q. Braster, M. Drechsler, M. J. Daemen, E. Lutgens, and O. Soehnlein, "Atherosclerotic plaque destabilization in mice: A comparative study," *PLoS ONE*, vol. 10, no. 10, Oct. 2015, Art. no. e0141019.

[52] M. Naghavi, "From vulnerable plaque to vulnerable patient: A call for new definitions and risk assessment strategies: Part I," *Circulation*, vol. 108, no. 14, pp. 1664–1672, Oct. 2003, doi: 10.1161/01.CIR.0000087480.94275.97.

[53] L. Pletsch-Borba, M. Selwaness, A. van der Lugt, A. Hofman, O. H. Franco, and M. W. Vernooij, "Change in carotid plaque components," *Cardiovascular Imag.*, vol. 11, no. 2, pp. 184–192, Feb. 2018, doi: 10.1016/j.jcmg.2016.12.026.

[54] R. J. Adrian and C.-S. Yao, "Pulsed laser technique application to liquid and gaseous flows and the scattering power of seed materials," *Appl. Opt.*, vol. 24, no. 1, pp. 44–52, 1985.

[55] R. Selzer, "Improved common carotid elasticity and intima-media thickness measurements from computer analysis of sequential ultrasound frames," *Atherosclerosis*, vol. 154, no. 1, pp. 185–193, Jan. 2001.

[56] J. Fromageau, J.-L. Gennisson, C. Schmitt, R. L. Maurice, R. Mongrain, and G. Cloutier, "Estimation of polyvinyl alcohol cryogel mechanical properties with four ultrasound elastography methods and comparison with gold standard testings," *IEEE Trans. Ultrason., Ferroelectr., Freq. Control*, vol. 54, no. 3, pp. 498–509, Mar. 2007, doi: 10.1109/tuffc.2007.273.

[57] S. Carlier, I. A. Kakadiaris, N. Dib, M. Vavuranakis, S. M. O'Malley, K. Gul, C. J. Hartley, R. Metcalfe, R. Mehran, C. Stefanadis, E. Falk, G. Stone, M. Leon, and M. Naghavi, "Vasa vasorum imaging: A new window to the clinical detection of vulnerable atherosclerotic plaques," *Current Atherosclerosis Rep.*, vol. 7, no. 2, pp. 164–169, Mar. 2005.

HONGYU KANG (Member, IEEE) was born in Liaoning, China, in 1992. He received the master's degree from the College of Medicine and Biological Information Engineering, Northeastern University, China, in 2015. He is currently a Research Assistant with the Shenzhen Institute of Advanced Technology (SIAT), Chinese Academy of Sciences. He has published a number of international conference papers and posters at the IEEE International Conference on Information and Automation (ICIA), the International Conference on Biomedical Ultrasound (ICBMU), and the Acoustical Society of China. His main research interests include ultrasonic elastography and shear wave elastography and developing advanced ultrasound techniques for measuring vascular biomechanics.

YANLING ZHANG received the bachelor's degree in clinical medicine from the Xiangya School of Medicine, Central South University, Changsha, China, in 2004, and the master's degree in imaging and nuclear medicine and the Ph.D. degree in internal medicine from Sun Yat-sen University, Guangzhou, China, in 2007 and 2014, respectively. Since 2007, she has been with the Department of Ultrasound, Third Affiliated Hospital, Sun Yat-sen University, for more than ten years. Her research interests include the clinical application of the new technology of ultrasound, including application of contrast-enhanced ultrasound, ultrasound of liver transplantation, evaluation of vascular wall and plaque by elastography, and early diagnosis of atherosclerosis. She has authored or coauthored more than 30 refereed research articles related to above research fields. She is principal investigator of two projects, including the National Natural Science Foundation Grant of China.

XIAOWEI HUANG (Member, IEEE) was born in Guangdong, China, in 1989. He received the bachelor's degree in electrical and information engineering and the master's degree in biomedical engineering from Southern Medical University, China, in 2012 and 2015, respectively, and the Ph.D. degree in pattern recognition and intelligent system from the University of Chinese Academy of Sciences, China, in 2019.

He is currently an Assistant Research Fellow with the Shenzhen Institute of Advanced Technology (SIAT), Chinese Academy of Sciences. He has published ten peer-reviewed articles in IEEE TRANSACTIONS ON BIOMEDICAL ENGINEERING, the IEEE TRANSACTIONS ON ULTRASONICS, FERROELECTRICS, AND FREQUENCY CONTROL, and *Ultrasound in Medicine and Biology*. His research interests include ultrasound neuromodulation and ultrasonic medical image processing.

LILI NIU (Member, IEEE) received the master's degree in biomedical engineering from Northeast University, China, in 2009, and the Ph.D. degree in computer application technology from the Chinese Academy of Sciences (CAS), in 2012. She is currently an Associate Professor with the Shenzhen Institute of Advanced Technology, CAS. Her main research interests include developing advanced biomedical ultrasound techniques for measuring vascular biomechanics, and ultrasound neuromodulation. She has published more than 30 peer-reviewed journals in the biomedical engineering field, and applied more than ten patents. She is a principal investigator of six projects, including the National Natural Science Foundation Grant of China, and so on.

HUI ZHANG received the master's degree in cardiovascular medicine and the Ph.D. degree in ultrasound medicine from Sun Yat-sen University, Guangzhou, China, in 2004 and 2010, respectively. He worked as a Cardiovascular Medicine Doctor for eight years. And he was worked with the Department of Ultrasound, Third Affiliated Hospital, Sun Yat-sen University, for 15 years. His research work focuses on the ultrasound application of cardiovascular diseases, early diagnosis of atherosclerosis, and fetal hearts. He has authored or coauthored more than 30 refereed research articles related to above research fields. He has participated in nine foundation items as a principal investigator or collaborator, since 2005.

LISHENG XU (Senior Member, IEEE) received the B.S. degree in electrical power system automation, the M.S. degree in mechanical electronics, and the Ph.D. degree in computer science and technology from the Harbin Institute of Technology, Harbin, China, in 1998, 2000, and 2006, respectively. He is currently a Full Professor with the Sino-Dutch Biomedical and Information Engineering School, Northeastern University, China. He has authored or coauthored 219 international research articles and holds 17 invention patents. His current research interests include medical signal and image processing, medical imaging, and pattern recognition.

Dr. Xu is the Director of the Theory and Education Professional Committee, China Medical Informatics Association. He is a Senior Member of the Chinese Society of Biomedical Engineering. He is a member of the Editor Board for many international journals, such as *Physiological Measurement*, *Biomedical Engineering Online*, and *Computers in Biology and Medicine*.

DEREK ABBOTT (Fellow, IEEE) was born in South Kensington, London, U.K., in 1960. He received the B.Sc. degree (Hons.) in physics from Loughborough University, Leicestershire, U.K., in 1982, and the Ph.D. degree in electrical and electronic engineering from The University of Adelaide, Adelaide, SA, Australia, in 1995, under the supervision of K. Eshraghian and B. R. Davis.

From 1978 to 1986, he was a Research Engineer with the GEC Hirst Research Centre, London. From 1986 to 1987, he was a VLSI Design Engineer with Austek Miscrosystems, Australia. Since 1987, he has been with the University of Adelaide, where he is currently a Full Professor with the School of Electrical and Electronic Engineering. His research interests include multidisciplinary physics and electronic engineering applied to complex systems, networks, biomedical engineering, stochastics, and biophotonics.

Dr. Abbott coedited *Quantum Aspects of Life* (Imperial College Press, 2008) and coauthored *Stochastic Resonance* (Cambridge University Press, 2008) and *Terahertz Imaging for Biomedical Applications* (Springer-Verlag, 2012). He is a Fellow of the Institute of Physics (IoP), U.K., and an Honorary Fellow of Engineers Australia. He has been an Editor and/or a Guest Editor for a number of journals, including the IEEE JOURNAL OF SOLID-STATE CIRCUITS, the *Journals of Optics B*, *Microelectrons Journal*, *PLOS One*, the PROCEEDINGS OF THE IEEE, and the IEEE PHOTONICS JOURNAL. He is currently on the Editorial Boards of IEEE ACCESS, *Nature's Scientific Reports*, *Royal Society Open Science*, and *Frontiers in Physics*. He has received a number of rewards, including the Tall Poppy Award for Science (2004), the Australian Research Council Future Fellowship (2012), the David Dewhurst Medal (2015), the Barry Inglis Medal (2018), and the M. A. Sargent Medal (2019) for eminence in engineering.